

Lattice study of an electroweak phase transition at $m_h \simeq 126$ GeV

M. Laine^a, G. Nardini^b, K. Rummukainen^c

^a*Institute for Theoretical Physics, Albert Einstein Center, University of Bern,
Sidlerstrasse 5, CH-3012 Bern, Switzerland*

^b*Faculty of Physics, University of Bielefeld, D-33501 Bielefeld, Germany*

^c*Department of Physics and Helsinki Institute of Physics,
University of Helsinki, P.O.Box 64, FIN-00014 Helsinki, Finland*

Abstract

We carry out lattice simulations of a cosmological electroweak phase transition for a Higgs mass $m_h \simeq 126$ GeV. The analysis is based on a dimensionally reduced effective theory for an MSSM-like scenario including a relatively light coloured SU(2)-singlet scalar, referred to as a right-handed stop. The non-perturbative transition is stronger than in 2-loop perturbation theory, and may offer a window for electroweak baryogenesis. The main remaining uncertainties concern the physical value of the right-handed stop mass which according to our analysis could be as high as $m_{\tilde{t}_R} \simeq 155$ GeV; a more precise effective theory derivation and vacuum renormalization than available at present are needed for confirming this value.

1. Introduction

One of the most important cosmological conundra is that we live in a Baryon Asymmetric Universe (BAU), meaning that very few antiprotons are seen in cosmic rays, although quarks and antiquarks are produced in almost equal measure at collider experiments. One of the possible explanations for BAU is called electroweak baryogenesis [1]: it makes use of the Higgs mechanism which is assumed to undergo a “first order” phase transition in the Early Universe. A phase transition of this type leads to thermal non-equilibrium, one of the necessary Sakharov conditions for explaining the BAU. The others (C, CP, and baryon number violation) are also part of the Standard Model and its simple extensions. The open issue, for any model, is whether these necessary conditions also amount to sufficient ones.

Although electroweak baryogenesis is by no means the only available scenario for generating the BAU, it is attractive in that it offers for a very restricted framework, being successful only for specific parameter values that can conceivably be probed at the LHC. A disadvantage is that a complete and reliable calculation of the BAU is theoretically demanding (for a recent review see ref. [2]). However, a crucial step, which by itself leads to strong constraints, is to prove the existence of a strong first-order electroweak phase transition. For this step, which is the topic of the present paper, uncertainties can be brought under control through a combination of analytic computations and large-scale lattice Monte Carlo simulations.

Lattice studies of variants of the electroweak phase transitions have a long history by now. They represent the only known systematic way of circumventing the infrared problem of thermal field theory [3] that limits the accuracy of perturbative evaluations. For instance, it was originally envisaged that electroweak baryogenesis could work even within the Standard Model [1], but nowadays it is known that this possibility is not realized in nature. An unambiguous reason is furnished by lattice simulations [4, 5]: unlike suggested by perturbation theory, the transition is a crossover for a Higgs mass compatible with either LEP or LHC [6, 7] bounds, which implies that the system does not deviate from equilibrium.¹

On the other hand, simple extensions of the Standard Model, particularly the Minimal Supersymmetric Standard Model (MSSM), might change the picture. Indeed, even though very strongly constrained by now [9, 10], realizing electroweak baryogenesis in the classic MSSM [11]–[20] (or in extensions of the Standard Model resembling MSSM at low energies [21]) seems not to be excluded [22, 23, 24]. In particular, if right-handed stops are sufficiently light and left-handed stops are heavy enough, the electroweak phase transition can be strong even for a (lighter CP-even) Higgs mass $m_h \simeq 126$ GeV [22, 25]. This assertion relies, however, on perturbation theory, whose accuracy cannot be taken for granted. There-

¹It is commonly believed that the Standard Model also contains too little CP violation to allow for electroweak baryogenesis, however this issue is harder to prove beyond doubt, cf. e.g. ref. [8] for recent work and references.

fore, to confirm or rule out the scenario, lattice Monte Carlo simulations appear welcome.

In the past, lattice analyses have extensively studied the electroweak phase transition within the MSSM. However, even the latest simulations [26] only focussed on a part of the MSSM parameter space that corresponds to a lightest Higgs mass $m_h \lesssim 115$ GeV. This seems to be excluded by the recent LHC data [27]. It thus appears well-motivated to repeat the lattice analysis for $m_h \simeq 126$ GeV, and this is the aim of the present study.

The paper is organized as follows. In sec. 2 we review the dimensionally reduced effective theory of the MSSM with a light right-handed stop, and choose a parameter region where perturbative calculations find a strong electroweak phase transition. Within this region, we select a parameter point with $m_h \simeq 126$ GeV where we analyze the phase transition on the lattice (sec. 3). The lattice results are compared with the perturbative ones in sec. 4. Finally, sec. 5 is dedicated to an outlook and conclusions.

2. Dimensionally reduced effective theory

For the benefit of an impatient reader, we start by summarizing the four-dimensional (4d) parameter values which the effective theory simulations are believed to correspond to (sec. 2.1). Subsequently the theoretical foundations and practical implementation of the dimensionally reduced (3d) effective theory construction are briefly reviewed (sec. 2.2).

2.1. Parameter values

The present study is based on lattice simulations as explained in ref. [26], and on analytic dimensional reduction and vacuum renormalization formulae as described in ref. [28]. The physics setting is different from what might appear ideal from today's perspective: in particular, the presence of a relatively light CP-odd Higgs mass $m_A \approx 150$ GeV, as well as of relatively light gluinos of mass $M_3 \lesssim 300$ GeV, were assumed in ref. [28]. Even though this setting is problematic because of light stop bounds (forbidding small M_3 [29]) and dark matter constraints (disfavouring light m_A [30]), it provides for a conservative framework to prove the existence of a strong first-order phase transition with $m_h \simeq 126$ GeV. Indeed, we expect to find a stronger transition for larger CP-odd Higgs mass (decreasing m_A weakens the transition [26, 31]). Having relativistic gluinos in the thermal bath increases the right-handed stop thermal mass by $\sim 20\%$ and consequently pushes the right-handed stop vacuum mass parameter to more negative values but, as we have checked by a resummed 1-loop estimate, does otherwise not significantly affect the phase diagram.

A major difference with respect to ref. [28] where a left-handed stop mass $m_Q \lesssim 1$ TeV was assumed, is that here we push m_Q to much larger values. This is needed to achieve $m_h \simeq 126$ GeV but, as pointed out in ref. [32], this induces large logarithms that were not

resummed in ref. [28]. Our evaluations of the Higgs and right-handed stop masses, m_h and $m_{\tilde{t}_R}$, as functions of the MSSM parameters, are therefore approximate.

Another important point is the renormalization scale at which the couplings appearing in the thermal mass corrections are evaluated. Following ref. [17], it was assumed in ref. [28] that the couplings run to a scale $\sim 2\pi T$ like in the Standard Model [33]. To crosscheck the argument requires carrying out a full 2-loop dimensional reduction computation, which is absent at present in the parameter range considered. The concrete consequence of the assumption of a scale $2\pi T \gg m_{\text{top}}$ is that the strong gauge coupling is quite small; this implies that the right-handed stop squared mass parameter, m_U^2 , does not need to be as negative as sometimes assumed; and subsequently, that the physical right-handed stop mass $m_{\tilde{t}_R} \simeq \sqrt{m_{\text{top}}^2 - \tilde{m}_U^2}$ (for $A_t \approx 0$ and $\tilde{m}_U^2 \equiv -m_U^2 > 0$) is larger.

To be reminded of these uncertainties, we tag the parameters mentioned, as well as the temperature, by a star in the following:

$$\tilde{m}_U^* , \quad m_Q^* , \quad m_h^* , \quad m_{\tilde{t}_R}^* , \quad T^* , \quad (2.1)$$

and similarly for the less significant parameters. These numbers are therefore *not* to be interpreted as precise physical values.

With these reservations, the dimensional reduction formulae and the notation are identical to refs. [26, 28]. (As a small point, explicit CP violation has been switched off for simplicity). The perturbative phase diagram is illustrated in fig. 1. For the parameter setting

$$\begin{aligned} \tilde{m}_U^* = 70.5 \text{ GeV} , \quad m_Q^* = 7 \text{ TeV} , \quad \mu^* = M_2^* = m_A^* = 150 \text{ GeV} , \\ \tan \beta^* = 15 , \quad A_t^*/m_Q^* = 0.02 , \end{aligned} \quad (2.2)$$

where μ^* , M_2^* , $\tan \beta^*$ and A_t^* are defined in a standard way (see e.g. ref. [28]), the perturbative calculation yields $v(T_c^*)/T_c^* = 0.9$ in Landau gauge, where $v(T_c^*)$ is the gauge-fixed expectation value of the lighter Higgs at the critical temperature T_c^* (the precise definitions of these observables are given in secs. 3 and 4).² Notably, at this parameter point the lightest Higgs pole mass is $m_h^* \simeq 126 \text{ GeV}$ within the 1-loop approximation [34].

Comparing with refs. [22, 25], the mass parameter \tilde{m}_U^* and critical temperature T_c^* evaluated at $m_Q^* = 7 \text{ TeV}$ are substantially smaller, and consequently the physical stop mass $m_{\tilde{t}_R}^*$ is larger. The difference seems to be related to running effects in the thermal mass corrections as mentioned above (the discrepancy is smaller at $m_Q^* = 1 \text{ TeV}$, but of course then m_h^* becomes unphysically light). It is our ultimate goal to improve the dimensional reduction and vacuum renormalization computations for the case of a very large m_Q^* , but unfortunately this requires a substantial amount of new work, which is postponed to future. If it turns out that our tagged parameters are close to the physical ones, in particular $m_{\tilde{t}_R} \simeq 155 \text{ GeV}$

²The vev normalization is $v(0) \simeq 246 \text{ GeV}$.

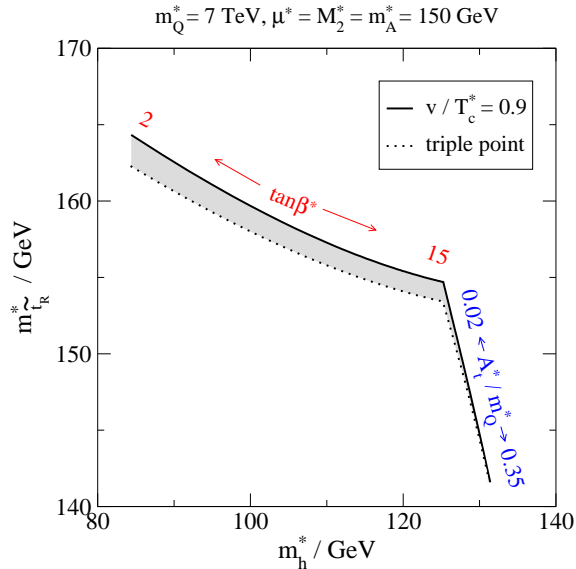


Figure 1: Slices of the perturbative phase diagram of the effective theory considered, in terms of the MSSM-like parameters defined in the text. The upper boundary corresponds to parameters at which $v(T_c^*)/T_c^*$ equals 0.9 in the Landau gauge; the lower boundary to values below which the theory is driven to a colour-broken minimum according to the 2-loop effective potential.

(cf. fig. 1), then the tension between LHC data and the considered MSSM scenario would be relaxed [9, 10, 22, 29]. (Note that since the transition we find is comfortably strong enough for baryogenesis, there remains some tolerance for a minor error in $m_{\tilde{t}_R}$.)

Despite the above uncertainties, there is still a well-defined problem to solve. Namely, we compare non-perturbative Monte Carlo simulations with 2-loop perturbation theory *within the 3d effective theory*. In other words, the effective parameters entering the simulations and the analytic formulae are identical. Therefore the finding of a non-perturbative effect in one or the other direction is likely to also persist with slightly modified parameter values.³ The actual simulations are carried out for the parameter values of eq. (2.2).

2.2. Review of theoretical setting

In order to appreciate the methods to be used, we briefly reiterate why it is non-trivial to determine reliably the properties of phase transitions even in weakly coupled theories. Technically, this is due to the so-called infrared problem of thermal field theory [3]. Let g denote a renormalized gauge coupling. Then the theory has three different momentum scales:

³The conclusions of our analysis also apply to models beyond the Standard Model that resemble the considered effective theory at low energies, for instance certain triplet extensions of the MSSM [21] or the Standard Model with an extra coloured scalar [35].

- The scale $p \sim 2\pi T$, technically originating from fields carrying non-zero Matsubara modes, is a “hard scale”; perturbation theory at this scale is free from infrared problems, and is expected to converge well (practical tests in the Standard Model suggest that after a 2-loop computation the remaining errors are on the percent level [36]).
- The scale $p \sim gT$, called the Debye or “soft” scale and technically originating from the interactions between the hard modes and the long-wavelength excitations, is also free from infrared problems. In general, perturbation theory at this scale converges slower than that at the hard scale, but in the electroweak theory there are very *many* hard modes, meaning that the Debye scale comes with a large numerical coefficient, making it in practice not much smaller than the scale $p \sim 2\pi T$. Indeed it has been checked (by comparing with full 4d simulations in an SU(2)+Higgs toy model [37]) that even the soft scale can be integrated out with good precision in the Standard Model [36].
- The “ultrasoft”, or “magnetic” scale $p \sim g^2 T/\pi$, first identified by Linde [3], is purely non-perturbative in nature, and needs to be studied numerically.

In the presence of a Higgs phase, the W^\pm, Z^0 bosons have masses $m_W, m_Z \simeq gv(T)/2$. If $v(T) \sim T$, then m_W, m_Z are formally “soft” scales and perturbation theory may or may not work, depending on numerical coefficients. However, if $v(T) \lesssim gT$, as is the case on the side of the high-temperature phase, then perturbation theory certainly breaks down. Therefore, in the following, m_W and m_Z are treated as ultrasoft scales.

Now, even though a scale hierarchy of the type described is a problem for perturbation theory (as it happens, it is also a challenge for direct 4d lattice simulations), it is a blessing once the problem is rephrased in an effective field theory language. Indeed the hard and soft scales *can* be integrated out perturbatively; it is only the ultrasoft scale which needs to be studied with lattice simulations. The integration out is called dimensional reduction [38, 39], and the lattice simulations are then those of purely bosonic 3d gauge+Higgs theories.

It is worth stressing that even if *no* simulations were carried out, it would nevertheless be useful to organize the computation in the above language. The reason is that the integrations over the hard and soft scales implement all-orders resummations (such as the “daisy” one), which are in fact necessary even for observables not sensitive to the ultrasoft scale.

With this background, the general steps of the adopted approach are as follows:

- **Derivation of a 3d effective theory.** The first step is to integrate out the hard and soft scales. To be specific, this step involves not only the actual finite-temperature calculations but also the corresponding vacuum computations, in order to express the $\overline{\text{MS}}$ scheme parameters in terms of experimentally measurable quantities.
- **2-loop perturbation theory within 3d effective theory.** Once an effective theory is available, it can first be studied with 2-loop perturbation theory. This is the

level that previous experience from the Standard Model and MSSM has shown to be semi-quantitatively accurate, *provided* that the transition is strong enough. Analytic expressions also yield a qualitative understanding of various parametric dependences.

- **Lattice formulation of 3d effective theory.** The derivation of the effective theory and its 2-loop perturbative analysis are, as a rule, carried out in a continuum regularization scheme, such as the $\overline{\text{MS}}$ scheme. Obviously, a lattice provides for a regularization scheme of its own. For a systematic study, the two schemes need to be related to each other; the principal relations have been worked out for a large class of theories [40].
- **Numerical simulations within 3d effective theory.** The last step of the program is to carry out lattice simulations. Although these are substantially simpler than full 4d simulations, they do remain non-trivial: infinite-volume and continuum limits need to be carefully taken in order to obtain physical results.

Without going into further details, which have been explained in refs. [26, 41], we recall the continuum form of the 3d theory simulated. The theory contains two Higgs SU(2) doublets, H_1 and H_2 , and a field U which is SU(2) singlet but SU(3) triplet. The Lagrangian has then the most general form allowed by symmetries,

$$\begin{aligned}
\mathcal{L}_{\text{3d}} T^* \equiv & \frac{1}{2} \text{Tr} G_{ij}^2 + (D_i^s U)^\dagger (D_i^s U) + m_U^2 (T^*) U^\dagger U + \lambda_U (U^\dagger U)^2 \\
& + \gamma_1 U^\dagger U H_1^\dagger H_1 + \gamma_2 U^\dagger U \tilde{H}_2^\dagger \tilde{H}_2 + [\gamma_{12} U^\dagger U H_1^\dagger \tilde{H}_2 + \text{H.c.}] \\
& + \frac{1}{2} \text{Tr} F_{ij}^2 + (D_i^w H_1)^\dagger (D_i^w H_1) + (D_i^w H_2)^\dagger (D_i^w H_2) \\
& + m_1^2 (T^*) H_1^\dagger H_1 + m_2^2 (T^*) \tilde{H}_2^\dagger \tilde{H}_2 + [m_{12}^2 (T^*) H_1^\dagger \tilde{H}_2 + \text{H.c.}] \\
& + \lambda_1 (H_1^\dagger H_1)^2 + \lambda_2 (\tilde{H}_2^\dagger \tilde{H}_2)^2 + \lambda_3 H_1^\dagger H_1 \tilde{H}_2^\dagger \tilde{H}_2 + \lambda_4 H_1^\dagger \tilde{H}_2 \tilde{H}_2^\dagger H_1 \\
& + [\lambda_5 (H_1^\dagger \tilde{H}_2)^2 + \lambda_6 H_1^\dagger H_1 H_1^\dagger \tilde{H}_2 + \lambda_7 \tilde{H}_2^\dagger \tilde{H}_2 H_1^\dagger \tilde{H}_2 + \text{H.c.}] , \tag{2.3}
\end{aligned}$$

where a factor T^* has been inserted in order to keep 4d dimensionalities of fields and couplings; D_i^s , D_i^w are the SU(3) and SU(2) covariant derivatives; G_{ij} , F_{ij} the corresponding field strength tensors; and $\tilde{H}_2 = i\sigma_2 H_2^*$. The hypercharge coupling has been set to zero, so there is only a global U(1) symmetry. The gauge couplings are denoted by g_w^2 and g_s^2 for SU(2) and SU(3), respectively. The actual values corresponding to the setting of eq. (2.2) are

$$m_1^2(T^*) \approx 26504 \text{ GeV}^2 + 0.1311(T^*)^2 , \tag{2.4}$$

$$m_2^2(T^*) \approx -4004 \text{ GeV}^2 + 0.6311(T^*)^2 , \tag{2.5}$$

$$m_{12}^2(T^*) \approx -1481 \text{ GeV}^2 - 0.0133(T^*)^2 , \tag{2.6}$$

$$m_U^2(T^*) \approx -4958 \text{ GeV}^2 + 0.8607(T^*)^2 , \tag{2.7}$$

$$\gamma_1 \approx -0.0031 , \quad \gamma_2 \approx 0.9995 , \quad \gamma_{12} \approx -0.0018 , \quad \lambda_U \approx 0.2020 , \tag{2.8}$$

β_w	volumes
8	$12^3, 16^3$
10	16^3
12	$16^3, 20^3, 32^3, 12^2 \times 36, 20^2 \times 40$
14	$24^3, 14^2 \times 42, 24^2 \times 48$
16	$24^3, 16^2 \times 48, 20^2 \times 60, 24^2 \times 72$
20	$32^3, 20^2 \times 60, 26^2 \times 72, 32^2 \times 64$
24	$24^3, 32^3, 48^3, 24^2 \times 78, 30^2 \times 72$
30	48^3

Table 1: The simulation volumes used in multicanonical simulations at temperatures around T_c^* .

$$\lambda_1 \approx 0.0649, \quad \lambda_2 \approx 0.1491, \quad \lambda_3 \approx 0.0589, \quad \lambda_4 \approx -0.1784, \quad (2.9)$$

$$\lambda_5 \approx 0.00009, \quad \lambda_6 \approx -0.00113, \quad \lambda_7 \approx -0.00117, \quad (2.10)$$

$$g_w^2 \approx 0.418, \quad g_s^2 \approx 1.085. \quad (2.11)$$

As can be seen from eqs. (2.5), (2.7), it is the fields \tilde{H}_2 and U that “drive” the transition; correspondingly, the couplings γ_2 , λ_U , and λ_2 are the most significant ones.

3. Lattice simulations

3.1. Action and algorithms

The theory in eq. (2.3) is discretized in the standard way, and for implementation details, we refer to refs. [26, 41]. For the gauge action we use the usual single plaquette Wilson formulation, with SU(2) and SU(3) lattice couplings $\beta_w = 4/(g_w^2 T^* a)$ and $\beta_s = 6/(g_s^2 T^* a)$. Here a is the lattice spacing, which we parameterize through β_w from now on.

Only the bare mass terms require renormalization in a 3d super-renormalizable theory:

$$m_{\text{latt}}^2 = m^2 + \Delta m^2. \quad (3.1)$$

Here m^2 stands for either m_U^2, m_1^2, m_2^2 or m_{12}^2 in the $\overline{\text{MS}}$ scheme, and Δm^2 is the counterterm containing the linear and logarithmic in a divergences [26]. With this renormalization only $O(a)$ cutoff errors remain, and the continuum limit can be taken by performing simulations at different β_w and by extrapolating $\beta_w \rightarrow \infty$ afterwards.

The update algorithm is a combination of heat bath and overrelaxation updates, with one compound update sweep consisting of one heat bath and three overrelaxation sweeps. The measurements are performed and recorded every two compound update steps.

It turns out that at the critical temperature the transition is strongly of first order, and the system does not spontaneously tunnel from one metastable phase to another with stan-

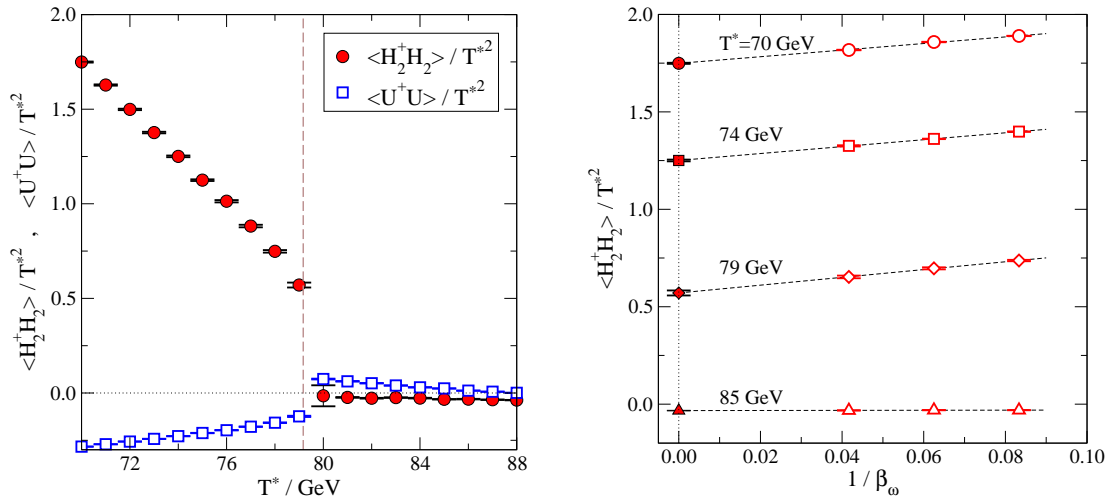


Figure 2: Left panel: the expectation values of $\langle H_2^\dagger H_2 \rangle$ and $\langle U^\dagger U \rangle$ as functions of the temperature T^* in the continuum limit. The vertical dashed line shows the phase transition temperature. Right panel: continuum extrapolation of $\langle H_2^\dagger H_2 \rangle$ at four chosen temperatures.

standard simulation algorithms. However, the probability distribution at the tunnelling region needs to be accurately resolved in order to precisely determine the critical temperature, the order parameter discontinuities, and the surface tension. We handle the strong metastability through the use of the *multicanonical* simulation method with automatic weight function calculation, combined with reweighting of the simulation temperature. We use the average $H_2^\dagger H_2$ as the multicanonical order parameter since this condensate is the most sensitive to the phase transition (H_1 is practically inert due to the large value $\tan \beta^* = 15$). The volumes simulated are listed in table 1.

3.2. Observables and results

The observables measured on the lattice are all extracted from gauge-invariant operators and are therefore gauge-independent by construction. Here we reiterate their definitions and show the main results.

Condensates as functions of the temperature: In order to obtain an overall view of the behaviour of the condensates $\langle H_i^\dagger H_i \rangle$ and $\langle U^\dagger U \rangle$ we perform a series of simulations at $T^* = 70\text{--}90$ GeV at three different lattice spacings, $\beta_w = 12, 16$ and 24 . The values of these condensates in the $\overline{\text{MS}}$ scheme with the scale parameter $\bar{\mu} = T^*$ are obtained by subtracting lattice divergences, for instance

$$\frac{\langle H_2^\dagger H_2 \rangle}{(T^*)^2} = \frac{\langle H_2^\dagger H_2 \rangle_{\text{latt}}}{(T^*)^2} - \frac{\Sigma}{2\pi a T^*} - \frac{3g_w^2}{16\pi^2} \left[\log \frac{6}{aT^*} + 0.66796 \right] + O(a), \quad (3.2)$$

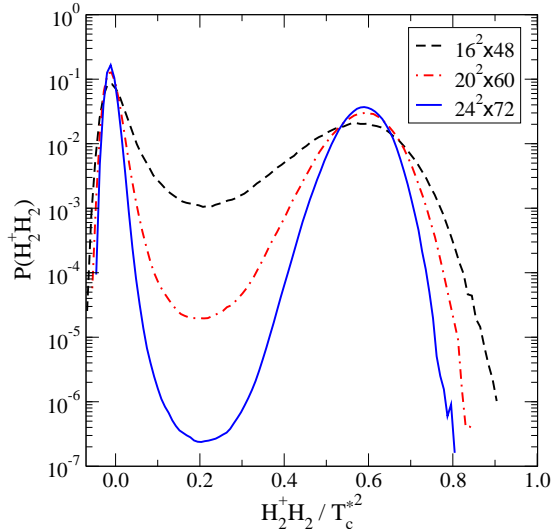


Figure 3: The volume-averaged probability distribution of $H_2^\dagger H_2$ at three different volumes with $\beta_w = 16$ and at $T_{c,\beta_w=16}^*$. As the volume increases, the probability density between the two peaks decreases exponentially.

where $\Sigma = 3.1759\dots$ originates from a 3d lattice tadpole integral. Here and in the following, we refer to the condensates with their original 4d dimensionalities. For our parameter settings, the values of these condensates extrapolated to the continuum are shown in the left panel of fig. 2. The figure highlights a first-order phase transition at a temperature around 80 GeV (the transition temperature as determined with separate multicanonical simulations is indicated with the vertical dashed line; see discussion below). The stop field U is also affected by the transition, due to its strong coupling to H_2 .

On the right panel we show the continuum extrapolation at four selected temperatures. The lattice divergences have been subtracted according to eq. (3.2), whereas the remnant $\mathcal{O}(a)$ effects have been eliminated by a linear extrapolation in $1/\beta_w$.

Critical temperature (T_c^*): The critical temperature is defined by the value of T^* at which two phases, identified through the expectation value of $\langle H_2^\dagger H_2 \rangle$, are equally likely to exist. Because the tunneling between the two phases is strongly suppressed (it is exponentially suppressed at large volumes, cf. eq. (3.8)), multicanonical simulations are implemented to overcome the tunneling barrier.

In our case the critical temperature is expected to be at around 80 GeV, as already indicated by fig. 2. Near this temperature we therefore run multicanonical simulations for the volumes and lattice spacings listed in table 1. For most of the lattice spacings, several volumes are used, enabling us to crosscheck the absence of finite-volume effects. The number of measurements at each volume is around $(0.5 - 2) \times 10^6$. Cylindrical volumes are needed for the surface

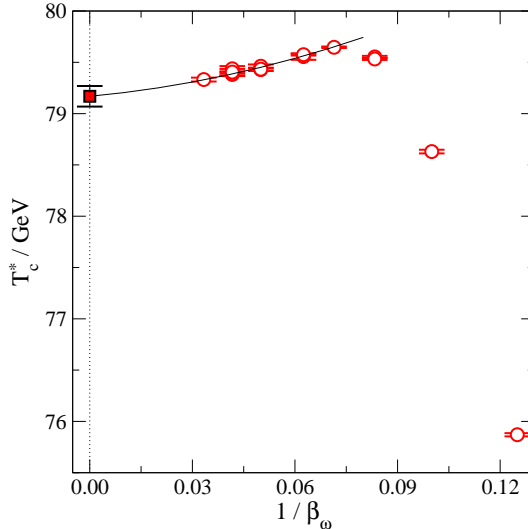


Figure 4: The critical temperature as a function of the lattice spacing $1/\beta_w$. With the volumes shown in table 1 no systematic volume dependence is seen, and all volumes are included in the plot. The interpolating curve is a second-order polynomial in a , fit to the points $\beta_w \geq 14$.

tension measurement, as described below.

As an example, the distribution of the volume-average of $H_2^\dagger H_2$, resulting from the simulations performed at $\beta_w = 16$, is shown in fig. 3. Clearly, the probability of configurations between the two phase peaks becomes strongly suppressed as the volume increases. The temperature has been reweighted from the simulation temperature ($T^* = 79.5$ GeV) to the apparent critical temperature where the area of the peaks is equal. The critical temperature averaged over all three volumes is $T_{c,\beta_w=16}^* \simeq 79.57$ GeV.

All the critical temperatures obtained for the lattice spacings and volumes of table 1 are summarized in fig. 4. A clear dependence on the lattice spacing is present, but results tend to stabilize as the continuum limit is approached. We then fit only data at $\beta_w \geq 14$ by a second-order polynomial in $1/\beta_w$. The continuum intercept reads

$$T_c^* = 79.17 \pm 0.10 \text{ GeV} , \quad (3.3)$$

with $\chi^2/\text{d.o.f.} = 11.2/8$ for the fit.

In fig. 5 the joint probability distribution of the volume-averaged $H_2^\dagger H_2$ and $U^\dagger U$ is shown. Clearly, the condensates move together: when $H_2^\dagger H_2$ becomes large, this effectively increases the mass of the U -field through the interaction mediated by the coupling γ_2 in eq. (2.3), and therefore its fluctuations become smaller. In fact in the $\overline{\text{MS}}$ scheme with the scale choice $\bar{\mu} = T^*$ the value of $\langle U^\dagger U \rangle$ becomes slightly negative at low temperatures, but this simply means that U is tightly confined into its “symmetric” phase in this regime.⁴

⁴It is in principle possible that separate symmetric \leftrightarrow broken H_2 and U phase transitions exist, giving rise

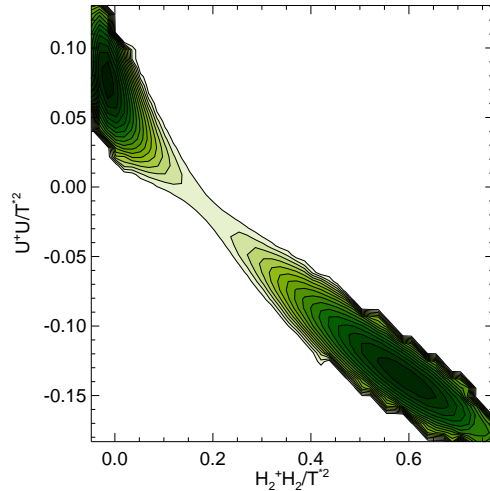


Figure 5: Contour plot of the joint probability distribution of the volume-averaged $H_2^\dagger H_2$ and $U^\dagger U$ at T_c^* . The measurement is for $\beta_w = 20$, volume = $32^2 \times 64$. The $\overline{\text{MS}}$ scheme value of $\langle U^\dagger U \rangle$ is slightly negative in the low-temperature phase (cf. the text).

Higgs discontinuity ($v(T_c^*)$): The Higgs discontinuity is defined on the lattice in a gauge-invariant and scale-independent manner as

$$\left(\frac{v^2(T_c^*)}{2} \right)_{\text{latt}} \equiv \Delta \left\langle \sum_{i=1}^2 H_i^\dagger H_i \right\rangle. \quad (3.4)$$

The quantity $\Delta \langle \cdot \rangle \equiv \langle \cdot \rangle_{\text{broken}} - \langle \cdot \rangle_{\text{symmetric}}$ is measured from the probability distributions at the critical temperature (such as those shown in fig. 3) by integrating over the peaks independently.⁵ In our case, the contribution of H_1 can be neglected since $\tan \beta^* \gg 1$.

The Higgs discontinuity as a function of the lattice spacing is shown in fig. 6 (left panel). Each point is obtained by averaging over the volumes listed in table 1. In this case $v(T_c^*)/T_c^*$ levels off almost completely at small enough lattice spacing, and a linear fit to points with $\beta_w \geq 16$ gives

$$\frac{v(T_c^*)}{T_c^*} = 1.117 \pm 0.005, \quad (3.5)$$

with $\chi^2/\text{d.o.f.} = 2.8/3$.

to three phases: fully symmetric, broken H_2 , and broken U . This has indeed been observed in a different parameter region, see fig. 9 of ref. [26]. However, in the case at hand we do not observe a stable broken U phase (no scan in \tilde{m}_U^* has been performed here).

⁵This involves setting a “separatrix” between the two phases, which is chosen to lie at the minimum of the probability distribution. As can be deduced from fig. 3, the ambiguity related to the choice becomes exponentially insignificant at large volumes.

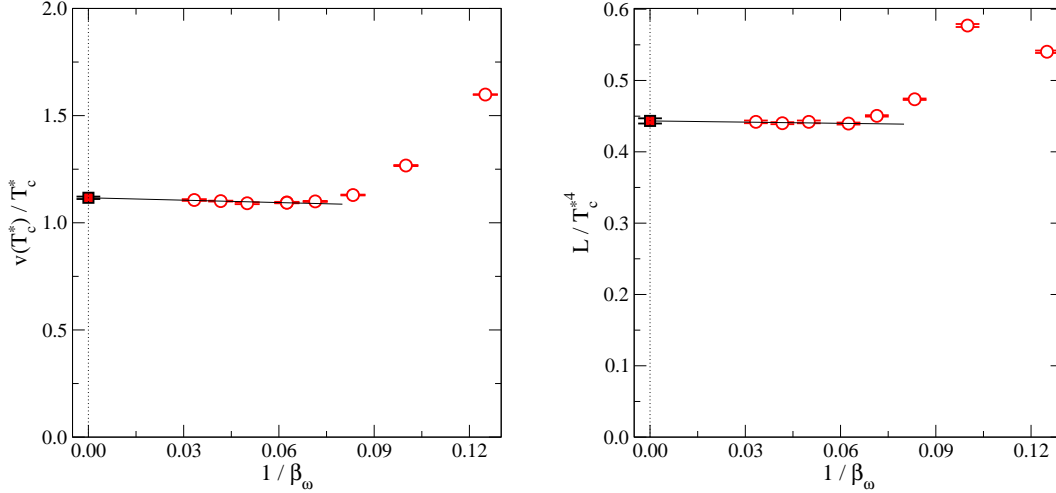


Figure 6: The Higgs discontinuity (left panel) and the latent heat (right panel) as functions of the lattice spacing. The linear continuum fit to points at $\beta_w \geq 16$ (solid line) is also shown.

The value of $v(T_c^*)/T_c^*$ is large enough so that the sphaleron rate (which is proportional to the baryon number violation rate) after the phase transition is negligible. Nevertheless, it should be stressed that $v(T^*)$ as defined by eq. (3.4) is a purely thermodynamic quantity, and therefore is not *equivalent* in any strict sense to the sphaleron rate. However, as non-perturbative real-time simulations for the Standard Model have shown [42], the value of $v(T_c^*)/T_c^*$ is *strongly correlated* with the sphaleron rate. Given the fact that non-perturbative real-time simulations are very expensive, only $v(T_c^*)/T_c^*$ is measured in the present study.

Latent heat (L): The latent heat is defined as the discontinuity of the energy density across a first order phase transition. It plays an essential role in the real-time hydrodynamics of bubble nucleation and growth. Within the approximate parametrization of the 3d theory used in this work, in which only mass parameters depend “non-conformally” on the temperature [cf. eqs. (2.4)–(2.11)], it can be measured as

$$\begin{aligned} \frac{L}{(T_c^*)^3} &= \Delta \left\langle U^\dagger U \frac{d}{dT^*} \left[\frac{m_V^2(T^*)}{(T^*)^2} \right] + \sum_{i=1}^2 H_i^\dagger H_i \frac{d}{dT^*} \left[\frac{m_i^2(T^*)}{(T^*)^2} \right] \right. \\ &\quad \left. + \left(H_1^\dagger \tilde{H}_2 \frac{d}{dT^*} \left[\frac{m_{12}^2(T^*)}{(T^*)^2} \right] + \text{H.c.} \right) \right\rangle. \end{aligned} \quad (3.6)$$

The discontinuity in eq. (3.6) is readily measured from multic canonical simulations, with the results shown on the right panel of fig. 6. The continuum limit gives

$$\frac{L}{(T_c^*)^4} = 0.443 \pm 0.004, \quad (3.7)$$

with $\chi^2/\text{d.o.f} = 1.01/2$ using a linear fit to data with $\beta_w \geq 16$.

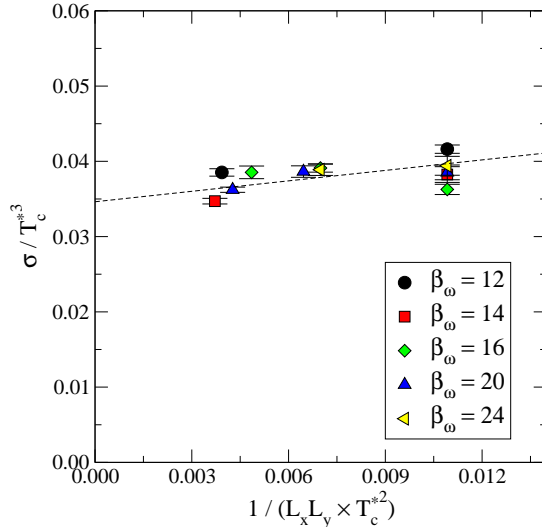


Figure 7: The surface tension of the interface between the symmetric and broken Higgs phases, plotted versus the inverse area of the interface.

Surface tension (σ): The surface tension is defined as the additional free energy per area carried by an interface between the two co-existing phases. This means that, in the large-volume limit, the probability of a configuration which contains an interface of area A , denoted by P_{\min} , is smaller than the probability of a configuration without interfaces, P_{\max} , by a factor

$$\frac{P_{\min}}{P_{\max}} = \exp\left(-\frac{\sigma A}{T^*}\right). \quad (3.8)$$

When the volume is finite, there are corrections to this relation, and properly accounting for these accelerates the convergence to the infinite-volume limit (cf. refs. [26, 41] for details).

The probabilities P_{\min} and P_{\max} can be directly read from the distributions in fig. 3: P_{\max} is the average peak height and P_{\min} is the minimum between the peaks. Because of the periodic boundary conditions the configurations here contain (at least) two interfaces. In practice it is advantageous to use lattice volumes where one dimension is longer than the other two, e.g. cylindrical volumes ($L_z \gg L_x, L_y$). In this case the interfaces are oriented transversely to the long direction ($A \approx 2L_x L_y$).

In fig. 7 measurements of the surface tension at each of the cylindrical volumes and lattice spacings indicated in table 1 are shown. In this case we are not able to obtain independently reliable (i.e. with small $\chi^2/\text{d.o.f}$) infinite volume and continuum limit extrapolations. This is likely due to still remaining finite volume effects; surface tension measurements are notoriously sensitive to volume. However, it is clear from the plot that the measurements settle down on a narrow band, independently of the lattice spacing. Extrapolating the band to the infinite

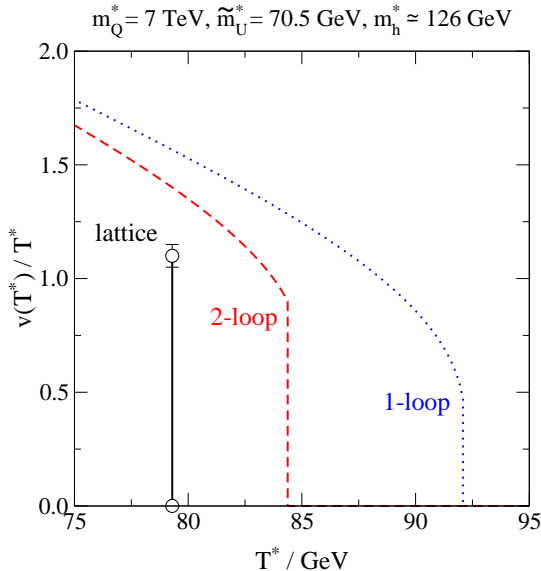


Figure 8: Comparison of perturbative and lattice results for the properties of the phase transition (here $v(T^*)$ refers, strictly speaking, to different quantities on the two sides; cf. sec. 4.2).

volume we cite a conservative but unprecise estimate of the error:

$$\frac{\sigma}{(T_c^*)^3} = 0.035 \pm 0.005 . \quad (3.9)$$

4. Comparison with perturbation theory

With a view of learning about generic features of the dynamics of the theory, probably applicable also to other parameter values than the very ones considered here but nevertheless close to $m_h \simeq 126 \text{ GeV}$, we proceed to comparing the lattice results with those of 2-loop perturbation theory within the 3d theory. We stress that since both results are based on the *same* 3d theory, the comparison is *not* jeopardized by perturbative uncertainties in dimensional reduction and vacuum renormalization as discussed in sec. 2.1. Indeed, these ultraviolet features play a role only in the relation of the approximate parameters ($T^*, m_h^*, m_{\tilde{t}_R}^*$, etc) to the physical ones ($T, m_h, m_{\tilde{t}_R}$, etc). For conceptual clarity, we furthermore split the comparison into two parts, given that some of the perturbative numbers cited are specific to Landau gauge, in accordance with established (although not necessary) conventions of the field.

4.1. Identical observables

Two of the observables, namely the critical temperature and latent heat, have definitions [see eq. (3.6) for the latter] that can be operatively applied both to lattice and perturbative

calculations. Their values for the case analyzed are

$$\frac{T_c^*}{\text{GeV}} = 79.17(10) \quad (\text{latt}), \quad \frac{T_c^*}{\text{GeV}} = 84.4 \quad (\text{pert}), \quad (4.1)$$

$$\frac{L}{(T_c^*)^4} = 0.443(4) \quad (\text{latt}), \quad \frac{L}{(T_c^*)^4} = 0.26 \quad (\text{pert}). \quad (4.2)$$

For the critical temperature the situation is illustrated in fig. 8. As has been observed also in the past [26], the main qualitative effect from non-perturbative dynamics is that the critical temperature is lowered. The latent heat is enhanced by $\sim 50\%$.

4.2. Correlated observables

Within 2-loop perturbation theory, the gauge-independent observable defined by eq. (3.4) happens to be very close to the gauge-fixed Higgs vev as computed in Landau gauge. Due to the fact that the Landau-gauge convention continues to be widespread in the literature, we therefore compare the lattice number directly with the Landau-gauge perturbative result:

$$\left(\frac{v}{T_c^*}\right)_{\text{eq. (3.4)}} = 1.117(5) \quad (\text{latt}), \quad \left(\frac{v}{T_c^*}\right)_{\text{Landau}} = 0.9 \quad (\text{pert}). \quad (4.3)$$

The percentual strengthening effect is smaller than for L , because L is essentially quadratic in v (cf. eq. (3.6)). Another quantity for which we are influenced by convention and ease of computation is the surface tension; this is usually extracted from the Landau gauge effective potential, with tree-level kinetic terms employed in finding the saddle point solution (for a recent discussion, see ref. [43]). The comparison reads

$$\left(\frac{\sigma}{(T_c^*)^3}\right)_{\text{eq. (3.8)}} = 0.035(5) \quad (\text{latt}), \quad \left(\frac{\sigma}{(T_c^*)^3}\right)_{\text{Landau}} = 0.025 \quad (\text{pert}). \quad (4.4)$$

5. Discussion and conclusions

The recent LHC discovery of a Higgs-like boson with a mass of around 126 GeV may have provided crucial information for electroweak baryogenesis. In many models beyond the Standard Model, the success of electroweak baryogenesis in explaining the baryon asymmetry of the Universe is indeed very sensitive to the Higgs mass through the requirement of a strong first-order electroweak phase transition. In the MSSM, perturbative studies have suggested that a strong first-order electroweak phase transition may exist even at $m_h \simeq 126$ GeV [22, 25]. However, since the transition is not exceedingly strong and the side of the “symmetric” phase is purely non-perturbative in nature, it is not clear whether the perturbative predictions are quantitatively accurate. In this paper we have studied the infrared dynamics of the transition by simulating a dimensionally reduced effective theory numerically, and compared the

results with 2-loop perturbative calculations within the same effective theory. Unless there are unexpectedly large 2-loop corrections to the relations between the effective parameters of the dimensionally reduced theory and four-dimensional physical low-energy observables, the simulations correspond to an MSSM-like parameter point with $m_h \simeq 126$ GeV and $m_{\tilde{t}_R} \simeq 155$ GeV, with larger uncertainties on the latter. (The simulations, however, are expected to also cover other extensions of the Standard Model having a stop-like field at the electroweak scale, i.e. providing for a similar low-energy effective theory.)

In the lattice simulations carried out, we have consistently seen a stronger transition than in perturbation theory. Actually, despite the larger Higgs mass, the strengthening effect is more substantial than in ref. [26]. In some sense the system is driven towards a phase where the right-handed stop experiences very strong fluctuations (manifested by a large $\langle U^\dagger U \rangle$), and the transition to the electroweak minimum takes place “from there” (cf. fig. 5).⁶

For a precise understanding of baryogenesis, it is not enough to study the properties of the transition at the critical temperature, but issues such as supercooling, nucleation, and bubble dynamics need to be considered as well (see e.g. refs. [45]–[47] for recent discussions). The nucleation temperature, T_n , is well approximated by the classical estimate [48] if it is calculated with non-perturbative values of the latent heat and surface tension inserted [49]. After nucleation and bubble collisions, the latent heat released may also reheat the system towards the critical temperature, which would enhance baryon number washout.

Various scenarios for the real-time dynamics of the transition have been studied in ref. [50], and in fact the dynamics of the present transition is not unlike case (A) considered there. More precisely, reheating up to T_c would take place if

$$\frac{L}{T_c^4} \gtrsim 8 \left(\frac{\sigma}{T_c^3} \right)^{3/4}. \quad (5.1)$$

This is (narrowly) avoided according to eqs. (4.2) and (4.4). Moreover, supercooling is roughly

$$\frac{T_c - T_n}{T_c} \simeq 0.54 \left(\frac{\sigma}{T_c^3} \right)^{3/2} \left(\frac{T_c^4}{L} \right) \simeq 0.008. \quad (5.2)$$

It is therefore quite modest, and is not expected to change the Higgs vev substantially (cf. figs. 2, 8). However, modern hydrodynamics studies of the phase transition will make these conclusions firmer [51].

At the moment the physical 4d parameter values to which our simulations correspond, particularly the right-handed stop mass, contain uncertainties of several GeV. To remove this perturbative uncertainty, full 2-loop dimensional reduction and at least 1-loop on-shell vacuum renormalization computations (expressing $\overline{\text{MS}}$ scheme parameters in terms of physical low-energy observables), such as were carried out for the Standard Model [33], are needed.

⁶Considerations such as those in ref. [44] are evaded because this is not a perturbatively “colour-broken” phase and the transition to the physical vacuum does take place, as the estimate in eq. (5.2) shows.

Despite the encouraging results that we have found, it is also clear that an exclusion of light SU(2)-singlet stop-like particles at the LHC could easily rule out the MSSM-based electroweak baryogenesis scenario. Therefore, it may be worthwhile to apply the techniques of the present study to more general models. Very many possibilities can be envisaged; as an example of a relatively well-constrained one, let us mention the so-called Inert Doublet Model [52, 53], i.e. a particular version of the two-Higgs-Doublet Model with an imposed unbroken Z(2) symmetry which reduces the number of free parameters. This model has many attractive features, for instance the heavy Higgs doublet could naturally serve as Dark Matter [54, 55]. The theory could conceivably lead to a strong first order phase transition as well [56, 57, 58], and a non-perturbative study may again be welcome.

Acknowledgements

K.R. acknowledges support from the Academy of Finland project 1134018. Simulations were carried out at the University of Helsinki and at the Finnish IT Center for Science (CSC).

References

- [1] V.A. Kuzmin, V.A. Rubakov and M.E. Shaposhnikov, *On the Anomalous Electroweak Baryon Number Nonconservation in the Early Universe*, Phys. Lett. B 155 (1985) 36.
- [2] D.E. Morrissey and M.J. Ramsey-Musolf, *Electroweak baryogenesis*, 1206.2942.
- [3] A.D. Linde, *Infrared problem in thermodynamics of the Yang-Mills gas*, Phys. Lett. B 96 (1980) 289.
- [4] K. Kajantie, M. Laine, K. Rummukainen and M.E. Shaposhnikov, *Is there a hot electroweak phase transition at $m_H \gtrsim m_W$?*, Phys. Rev. Lett. 77 (1996) 2887 [hep-ph/9605288].
- [5] K. Rummukainen, M. Tsy-pin, K. Kajantie, M. Laine and M.E. Shaposhnikov, *The Universality class of the electroweak theory*, Nucl. Phys. B 532 (1998) 283 [hep-lat/9805013].
- [6] S. Chatrchyan *et al.* [The CMS Collaboration], *Observation of a new boson at a mass of 125 GeV with the CMS experiment at the LHC*, Phys. Lett. B 716 (2012) 30 [1207.7235].
- [7] G. Aad *et al.* [The ATLAS Collaboration], *Observation of a new particle in the search for the Standard Model Higgs boson with the ATLAS detector at the LHC*, Phys. Lett. B 716 (2012) 1 [1207.7214].

- [8] T. Brauner, O. Taanila, A. Tranberg and A. Vuorinen, *Computing the temperature dependence of effective CP violation in the Standard Model*, JHEP 11 (2012) 076 [1208.5609].
- [9] D. Curtin, P. Jaiswal and P. Meade, *Excluding Electroweak Baryogenesis in the MSSM*, JHEP 08 (2012) 005 [1203.2932].
- [10] T. Cohen, D.E. Morrissey and A. Pierce, *Electroweak Baryogenesis and Higgs Signatures*, Phys. Rev. D 86 (2012) 013009 [1203.2924].
- [11] M.S. Carena, M. Quirós and C.E.M. Wagner, *Opening the window for electroweak baryogenesis*, Phys. Lett. B 380 (1996) 81 [hep-ph/9603420].
- [12] J.R. Espinosa, *Dominant two loop corrections to the MSSM finite temperature effective potential*, Nucl. Phys. B 475 (1996) 273 [hep-ph/9604320].
- [13] D. Delepine, J.M. Gérard, R. Gonzalez Felipe and J. Weyers, *A Light stop and electroweak baryogenesis*, Phys. Lett. B 386 (1996) 183 [hep-ph/9604440].
- [14] J.M. Cline and K. Kainulainen, *Supersymmetric electroweak phase transition: Beyond perturbation theory*, Nucl. Phys. B 482 (1996) 73 [hep-ph/9605235].
- [15] M. Losada, *High temperature dimensional reduction of the MSSM and other multiscalar models*, Phys. Rev. D 56 (1997) 2893 [hep-ph/9605266].
- [16] M. Laine, *Effective theories of MSSM at high temperature*, Nucl. Phys. B 481 (1996) 43 [Erratum-ibid. B 548 (1999) 637] [hep-ph/9605283].
- [17] D. Bödeker, P. John, M. Laine and M.G. Schmidt, *The Two loop MSSM finite temperature effective potential with stop condensation*, Nucl. Phys. B 497 (1997) 387 [hep-ph/9612364].
- [18] B. de Carlos and J.R. Espinosa, *The Baryogenesis window in the MSSM*, Nucl. Phys. B 503 (1997) 24 [hep-ph/9703212].
- [19] J.M. Cline and G.D. Moore, *Supersymmetric electroweak phase transition: Baryogenesis versus experimental constraints*, Phys. Rev. Lett. 81 (1998) 3315 [hep-ph/9806354].
- [20] M. Losada, *The Two loop finite temperature effective potential of the MSSM and baryogenesis*, Nucl. Phys. B 537 (1999) 3 [hep-ph/9806519].
- [21] A. Delgado, G. Nardini and M. Quirós, *The Light Stop Scenario from Gauge Mediation*, JHEP 04 (2012) 137 [1201.5164].
- [22] M. Carena, G. Nardini, M. Quirós and C.E.M. Wagner, *MSSM Electroweak Baryogenesis and LHC Data*, 1207.6330.

- [23] D.J.H. Chung, A.J. Long and L.-T. Wang, *The 125 GeV Higgs and Electroweak Phase Transition Model Classes*, 1209.1819.
- [24] W. Huang, J. Shu and Y. Zhang, *On the Higgs Fit and Electroweak Phase Transition*, 1210.0906.
- [25] M. Carena, G. Nardini, M. Quirós and C.E.M. Wagner, *The Baryogenesis Window in the MSSM*, Nucl. Phys. B 812 (2009) 243 [0809.3760].
- [26] M. Laine and K. Rummukainen, *Two Higgs doublet dynamics at the electroweak phase transition: A Non-perturbative study*, Nucl. Phys. B 597 (2001) 23 [hep-lat/0009025].
- [27] A. Arbey, M. Battaglia, A. Djouadi and F. Mahmoudi, *An update on the constraints on the phenomenological MSSM from the new LHC Higgs results*, 1211.4004.
- [28] M. Laine and K. Rummukainen, *Higgs sector CP violation at the electroweak phase transition*, Nucl. Phys. B 545 (1999) 141 [hep-ph/9811369].
- [29] M. Lungwitz, *Search for third generation squarks with the ATLAS detector*, ATL-PHYS-PROC-2012-215 [cds.cern.ch/record/1483992].
- [30] J. Kozaczuk and S. Profumo, *Closing in on Supersymmetric Electroweak Baryogenesis with Dark Matter Searches and the Large Hadron Collider*, JCAP 11 (2011) 031 [1108.0393].
- [31] M.S. Carena, M. Quirós, A. Riotto, I. Vilja and C.E.M. Wagner, *Electroweak baryogenesis and low-energy supersymmetry*, Nucl. Phys. B 503 (1997) 387 [hep-ph/9702409].
- [32] M. Carena, G. Nardini, M. Quirós and C.E.M. Wagner, *The Effective Theory of the Light Stop Scenario*, JHEP 10 (2008) 062 [0806.4297].
- [33] K. Kajantie, M. Laine, K. Rummukainen and M.E. Shaposhnikov, *Generic rules for high temperature dimensional reduction and their application to the Standard Model*, Nucl. Phys. B 458 (1996) 90 [hep-ph/9508379].
- [34] J. Ellis, G. Ridolfi and F. Zwirner, *On radiative corrections to supersymmetric Higgs boson masses and their implications for LEP searches*, Phys. Lett. B 262 (1991) 477.
- [35] T. Cohen and A. Pierce, *Electroweak Baryogenesis and Colored Scalars*, Phys. Rev. D 85 (2012) 033006 [1110.0482].
- [36] M. Laine, *The Renormalized gauge coupling and non-perturbative tests of dimensional reduction*, JHEP 06 (1999) 020 [hep-ph/9903513].

- [37] F. Csikor, Z. Fodor and J. Heitger, *Endpoint of the hot electroweak phase transition*, Phys. Rev. Lett. 82 (1999) 21 [hep-ph/9809291].
- [38] P. Ginsparg, *First and second order phase transitions in gauge theories at finite temperature*, Nucl. Phys. B 170 (1980) 388.
- [39] T. Appelquist and R.D. Pisarski, *High-temperature Yang-Mills theories and three-dimensional Quantum Chromodynamics*, Phys. Rev. D 23 (1981) 2305.
- [40] M. Laine and A. Rajantie, *Lattice continuum relations for 3d $SU(N)$ +Higgs theories*, Nucl. Phys. B 513 (1998) 471 [hep-lat/9705003].
- [41] M. Laine and K. Rummukainen, *The MSSM electroweak phase transition on the lattice*, Nucl. Phys. B 535 (1998) 423 [hep-lat/9804019].
- [42] M. D'Onofrio, K. Rummukainen and A. Tranberg, *The Sphaleron Rate through the Electroweak Cross-over*, JHEP 08 (2012) 123 [1207.0685].
- [43] M. Garny and T. Konstandin, *On the gauge dependence of vacuum transitions at finite temperature*, JHEP 07 (2012) 189 [1205.3392].
- [44] J.M. Cline, G.D. Moore and G. Servant, *Was the electroweak phase transition preceded by a color broken phase?*, Phys. Rev. D 60 (1999) 105035 [hep-ph/9902220].
- [45] J.R. Espinosa, T. Konstandin, J.M. No and G. Servant, *Energy Budget of Cosmological First-order Phase Transitions*, JCAP 06 (2010) 028 [1004.4187].
- [46] S.J. Huber and M. Sopena, *The bubble wall velocity in the minimal supersymmetric light stop scenario*, Phys. Rev. D 85 (2012) 103507 [1112.1888].
- [47] A. Megevand and A.D. Sanchez, *Analytic approach to the motion of cosmological phase transition fronts*, Nucl. Phys. B 865 (2012) 217 [1206.2339].
- [48] L.D. Landau and E.M. Lifshitz, *Statistical Physics*, Third Edition, §162 (Butterworth-Heinemann, Oxford).
- [49] G.D. Moore and K. Rummukainen, *Electroweak bubble nucleation, non-perturbatively*, Phys. Rev. D 63 (2001) 045002 [hep-ph/0009132].
- [50] H. Kurki-Suonio and M. Laine, *Real-time history of the cosmological electroweak phase transition*, Phys. Rev. Lett. 77 (1996) 3951 [hep-ph/9607382].
- [51] M. Hindmarsh, S.J. Huber, K. Rummukainen and D.J. Weir, in preparation.

- [52] E. Ma, *Verifiable radiative seesaw mechanism of neutrino mass and dark matter*, Phys. Rev. D 73 (2006) 077301 [hep-ph/0601225].
- [53] R. Barbieri, L.J. Hall and V.S. Rychkov, *Improved naturalness with a heavy Higgs: An Alternative road to LHC physics*, Phys. Rev. D 74 (2006) 015007 [hep-ph/0603188].
- [54] L. Lopez Honorez, E. Nezri, J.F. Oliver and M.H.G. Tytgat, *The Inert Doublet Model: An Archetype for Dark Matter*, JCAP 02 (2007) 028 [hep-ph/0612275].
- [55] T. Hambye and M.H.G. Tytgat, *Electroweak symmetry breaking induced by dark matter*, Phys. Lett. B 659 (2008) 651 [0707.0633].
- [56] T.A. Chowdhury, M. Nemevsek, G. Senjanovic and Y. Zhang, *Dark Matter as the Trigger of Strong Electroweak Phase Transition*, JCAP 02 (2012) 029 [1110.5334].
- [57] D. Borah and J.M. Cline, *Inert Doublet Dark Matter with Strong Electroweak Phase Transition*, Phys. Rev. D 86 (2012) 055001 [1204.4722].
- [58] G. Gil, P. Chankowski and M. Krawczyk, *Inert Dark Matter and Strong Electroweak Phase Transition*, Phys. Lett. B 717 (2012) 396 [1207.0084].